



## **Ozone and carbon monoxide budgets over the Eastern Mediterranean**

S. Myriokefalitakis, Nikolaos Daskalakis, G.S. Fanourgakis, A. Voulgarakis, M.C. Krol, J.M.J. Aan de Brugh, M. Kanakidou

### **► To cite this version:**

S. Myriokefalitakis, Nikolaos Daskalakis, G.S. Fanourgakis, A. Voulgarakis, M.C. Krol, et al.. Ozone and carbon monoxide budgets over the Eastern Mediterranean. *Science of the Total Environment*, 2016, 563-564, pp.40-52. <10.1016/j.scitotenv.2016.04.061>. <insu-01330364>

**HAL Id: insu-01330364**

**<https://insu.hal.science/insu-01330364v1>**

Submitted on 4 Mar 2021

**HAL** is a multi-disciplinary open access archive for the deposit and dissemination of scientific research documents, whether they are published or not. The documents may come from teaching and research institutions in France or abroad, or from public or private research centers.

L'archive ouverte pluridisciplinaire **HAL**, est destinée au dépôt et à la diffusion de documents scientifiques de niveau recherche, publiés ou non, émanant des établissements d'enseignement et de recherche français ou étrangers, des laboratoires publics ou privés.



HAL Authorization

# **Ozone and carbon monoxide budgets over the Eastern Mediterranean**

**S. Myriokefalitakis <sup>a</sup>, N. Daskalakis <sup>a,b,1</sup>, G. S. Fanourgakis <sup>a</sup>, A. Voulgarakis <sup>c</sup>, M. C. Krol <sup>d,e,f</sup>, J. M. J. Aan de Brugh <sup>f</sup> and M. Kanakidou <sup>a</sup>**

<sup>a</sup> Environmental Chemical Processes Laboratory (ECPL), Department of Chemistry, University of Crete, P.O. Box 2208, 70013 Heraklion, Greece

<sup>b</sup> Institute of Chemical Engineering, Foundation for Research and Technology Hellas (FORTH/ICE - HT), 26504 Patras, Greece

<sup>c</sup> Department of Physics, Imperial College London, London, UK

<sup>d</sup> Meteorology and Air Quality Section, Wageningen University, Wageningen, The Netherlands

<sup>e</sup> Institute for Marine and Atmospheric Research, Utrecht University, Utrecht, The Netherlands

<sup>f</sup> SRON Netherlands Institute for Space Research, Utrecht, The Netherlands

<sup>1</sup>now at: LATMOS, Laboratoire Atmosphères, Milieux, Observations Spatiales, UPMC/UVSQ/CNRS, Paris, France

Corresponding author: [stelios@uoc.gr](mailto:stelios@uoc.gr) (S. Myriokefalitakis); [mariak@uoc.gr](mailto:mariak@uoc.gr) (M. Kanakidou)

## 18   **Abstract**

19   The importance of the long-range transport (LRT) on O<sub>3</sub> and CO budgets over the Eastern  
20   Mediterranean has been investigated using the state-of-the-art 3-dimensional global chemistry-  
21   transport model TM4-ECPL. A 3-D budget analysis has been performed separating the Eastern  
22   from the Western basins and the boundary layer (BL) from the free troposphere (FT). The FT of  
23   the Eastern Mediterranean is shown to be a strong receptor of polluted air masses from the  
24   Western Mediterranean, and the most important source of polluted air masses for the Eastern  
25   Mediterranean BL, with about 40% of O<sub>3</sub> and of CO in the BL to be transported from the FT  
26   aloft. Regional anthropogenic sources are found to have relatively small impact on regional air  
27   quality in the area, contributing by about 8% and 18% to surface levels of O<sub>3</sub> and CO,  
28   respectively. Projections using anthropogenic emissions for the year 2050 but neglecting climate  
29   change calculate a surface O<sub>3</sub> decrease of about 11% together with a surface CO increase of  
30   roughly 10% in the Eastern Mediterranean.

31   **Keywords:** Ozone (O<sub>3</sub>), Carbon monoxide (CO), Eastern Mediterranean (EM), Long-range  
32   transport (LRT), Free Troposphere (FT)

33

## 1. Introduction

Tropospheric  $O_3$  and CO are atmospheric pollutants both generated from natural and anthropogenic sources depending on numerous physical and chemical processes (e.g. Lelieveld and Dentener, 2000). They significantly affect the oxidizing capacity of the troposphere, climate (IPCC, 2013) and human and ecosystem's health (e.g. Jimoda, 2012; Ainsworth et al., 2012; Yue and Unger, 2014). Therefore, much attention is been paid to limit exceedances of threshold air pollution levels set by Environmental policy directives (e.g. DIRECTIVE 2008/50/EC Annex VII). Attribution of air pollution to sources is a prerequisite for designing measures to be taken to comply with such instructions. Pollution within urban agglomerations can build-up both locally (via local emissions and chemistry) and regionally (via transport from other regions) (e.g. Parrish et al., 2011). In the outflow of pollution centers, oxidation of volatile organic compounds (VOCs) and CO fosters the formation of secondary pollutants such as  $O_3$  (Molina and Molina, 2002), which is produced during the oxidation of VOCs in the presence of nitrogen oxides ( $NO_x$ ) (Crutzen, 1974; Derwent et al., 1996; Monks et al., 2009) following non-linear chemical processes. Therefore, it is particularly important to know whether actions on national level or coordinated actions on regional, or even global scale, are needed to limit air pollution in a region.

In this respect, Colette et al. (2012) analyzed atmospheric pollutant surface observations in Europe to derive trends over the past decade and compared them with multi-model chemistry-transport simulations. They found robust decreases of  $NO_x$  throughout Europe except in South-Eastern France and North Italy and pointed out much larger model uncertainty over the Mediterranean than elsewhere. Over the Eastern Mediterranean (EM), they calculate a decrease in non-methane volatile organic compounds (NMVOC) to  $NO_x$  ratio indicating a shift in the chemical regime in the area. Beekmann and Vautard (2010) have shown that the Mediterranean atmosphere is a  $NO_x$  sensitive regime, while North-Western Europe is always VOC sensitive. Furthermore, modeling studies simulate high  $O_3$  concentrations in the summer, in agreement with the observed northern hemisphere summertime  $O_3$  maxima (Zanis et al., 2014). They also predict higher  $O_3$  levels in parts of the European continent as a result of a warmer climate in the near future (Langner et al., 2012; Zanis et al., 2014) and an increase in regional biogenic emissions, both of which lead to a summertime regional  $O_3$  increase by 1 ppb  $^{\circ}C^{-1}$  (Im et al., 2011). Within large agglomerations of the EM,  $O_3$  is significantly depressed through reaction

with NO, followed by HNO<sub>3</sub> formation, in particular during wintertime (Im and Kanakidou, 2012).

The Mediterranean is among the most climatically sensitive regions of Europe, often exposed to multiple stresses, such as simultaneous water shortage and air pollution exposure (IPCC, 2013). It is also a characteristic region of a strongly coupled atmosphere-ocean system, composed by two basins that differ in air circulation patterns (Millán et al., 2005; Kallos et al., 2007) – the eastern and the western part. EM is affected by several large agglomerations, including the two megacities (<http://www.newgeography.com>): Istanbul (13.6 M; Turkey) at the northeastern edge, Cairo (17.8 M; Egypt) at the southern edge of the basin, and one agglomeration, Athens, which gathers 40% (4 M) of Greece's total population. The rapid urbanization and the unique location of the EM as a cross-road of air masses affected by various pollution sources has turned air pollution into a challenging environmental problem in the area. Air masses from upwind locations carrying anthropogenic emissions, mainly from Europe, the Balkans and the Black Sea, meet with biomass burning (Sciare et al., 2008), biogenic (Liakakou et al., 2009) and other natural emissions (Gerasopoulos et al., 2011) from surrounding regions under sunny and warm conditions that enhance photochemical build-up of pollutants (Lelieveld et al., 2002; Kanakidou et al., 2011).

To quantify the impact of anthropogenic sources on air-quality of the region as the EM, the inter- and the intra- continental transport have to be considered and distinguished from the impact of the regional sources (HTAP, 2011). Such analysis remains challenging, due to the chemical complexity of atmospheric composition and the significant seasonal and interannual variability of meteorological conditions that affect transport patterns (e.g. driven by the North Atlantic Oscillation; Pausata et al., 2012). Thus, large-scale chemistry-transport models (CTMs) are more appropriate tools for studying LRT (e.g. HTAP, 2011) than mesoscale models in which inter- /intra-continental transport procedures are strongly driven by the imposed boundary conditions. Satellite observations of tropospheric O<sub>3</sub>, NO<sub>2</sub> and aerosol optical thickness (AOT) over the Mediterranean clearly show the regional tropospheric O<sub>3</sub> column maximum over the Mediterranean sea as well as the high NO<sub>2</sub> columns in the urban pollution centers that surround the basin (Kanakidou et al., 2011). Ground-based and satellite observations and numerical modeling reviewed by Kanakidou et al. (2011) point out that air pollution transported to the area is of similar importance to local sources for the background air pollution levels in the EM.

95 Indeed, Drori et al. (2012) calculated that transport of air masses from Eastern Europe and  
96 Turkey to the EM can contribute up to 50 % of surface CO in the area. Gerasopoulos et al.  
97 (2005) analyzing observations provided evidence that the main mechanism controlling the high  
98 background tropospheric O<sub>3</sub> levels in the EM is the long-range transport (LRT) from the  
99 European continent (mainly during summer) and the local photochemical O<sub>3</sub> build-up (especially  
100 under western flow and stagnant wind conditions). In line with these findings, Zanis et al. (2014)  
101 attributed the characteristic summertime tropospheric O<sub>3</sub> pool over the EM to enhanced  
102 downward transport from the upper troposphere and lower stratosphere that characterize the  
103 summertime circulation over this region.

104 In the present study we investigate the contribution of LRT on O<sub>3</sub> and CO budgets in the  
105 Mediterranean basin, using a global CTM, the TM4-ECPL, to conduct a source attribution of  
106 atmospheric composition changes. The relative impacts of regional anthropogenic, biomass  
107 burning and natural emissions to the air quality in the EM are evaluated. First, the model set-up  
108 and methodology followed are described. Then simulated O<sub>3</sub> and CO levels are compared with  
109 in-situ observations and satellite retrievals on a European and global level and model  
110 deficiencies are discussed. The importance of regional emissions and the strength of LRT for air  
111 quality are investigated based on sensitivity simulations and budget analysis. Projected changes  
112 resulting from anthropogenic emissions scenarios for 2050 are also discussed.

## 113 **2. Materials and Methods**

### 114 *2.1 Global Model Set-up*

115 The global CTM TM4-ECPL (Daskalakis et al., 2015 and references therein) is able to simulate  
116 oxidant chemistry, accounting for NMVOCs, as well as all major aerosol components, including  
117 inorganic aerosols such as sulfate (SO<sub>4</sub><sup>2-</sup>), nitrate (NO<sub>3</sub><sup>-</sup>), ammonium (NH<sub>4</sub><sup>+</sup>) using the  
118 ISORROPIA II thermodynamic model (Fountoukis and Nenes, 2007) and secondary organic  
119 aerosols (SOA). Compared to its parent TM4 model (van Noije et al., 2004), the present version  
120 includes a description of glyoxal and other oxygenated organics (Myriokefalitakis et al., 2008)  
121 and organic aerosols (Myriokefalitakis et al., 2010). The model also accounts for multiphase  
122 chemistry in clouds and aerosol water that affects SOA formation (Myriokefalitakis et al., 2011)  
123 and dust solubility (Myriokefalitakis et al., 2015). TM4-ECPL has been previously evaluated for  
124 its ability i) to compute atmospheric composition and uncertainties associated with the use of

different biomass burning emissions (Daskalakis et al., 2015), ii) to reproduce distributions of tropospheric O<sub>3</sub> and its precursors, as well as aerosols over Asia in summer 2008 as seen by satellite and by in-situ observations (Quennehen et al., 2015), iii) to simulate the concentrations of sulfate, black carbon (BC) and other aerosols in the Arctic (Eckhardt et al., 2015) and iv) to evaluate the air quality impacts of short-lived pollutants based on current legislation for the recent past and present (Stohl et al., 2015).

For the present study, year 2008 anthropogenic emissions of NMVOC, NO<sub>x</sub>, CO, SO<sub>2</sub>, NH<sub>3</sub>, OC and BC developed within the EU - FP7 ECLIPSE project (Stohl et al., 2015) have been used to drive the chemistry in the model. Methane (CH<sub>4</sub>) is calculated by nudging surface concentrations to NOAA flask observations representative of the year of simulation (currently available for the years 1989-2010; M. van Weele, personal communication, 2013). Since TM4-ECPL does not explicitly calculate stratospheric chemistry, upper boundary conditions derived from climatology records of stratospheric concentrations have been applied for O<sub>3</sub>, CH<sub>4</sub> and HNO<sub>3</sub>. Thus, stratospheric O<sub>3</sub> concentrations are nudged above 50hPa to the concentrations of the year of simulation based on the Multi-Sensor Reanalysis (MSR) climatology record, which is available for the years 1978-2008 (van der A et al., 2010). For stratospheric CH<sub>4</sub> concentrations, the monthly climatology based on the HALogen Occultation Experiment (HALOE) on board the Upper Atmosphere Research Satellite (UARS) (Groß and Russell III, 2005) is applied above 50 hPa. In the stratosphere, HNO<sub>3</sub> is nudged at 10 hPa using Sub-millimetre and Millimetre Radiometer (SMR) observations from the Odin satellite (Brohede et al., 2008). This approach enables a realistic representation of the concentrations of these compounds in the upper layers of the model and thus of the vertical exchanges between the stratosphere and the troposphere. Further detailed information on the model set up and the emission inventories used in the model is available in Daskalakis et al. (2015).

Here, TM4-ECPL is driven by ECMWF (European Center for Medium - Range Weather Forecasts) Interim re-analysis project (ERA-Interim) meteorology (Dee et al., 2011). Advection of the tracers in the model is parameterized using the slopes scheme (Russell and Lerner, 1981). Convective transport is parameterized based on the Tiedtke (1989) and Olivié (2004) scheme. The vertical diffusion is parameterized as described in Louis (1979). The basic model configuration used for this study (BASE simulation; see Table 1) has a horizontal resolution of 3° in longitude by 2° in latitude, 34 vertical hybrid layers from the surface up to 0.1 hPa and a

time-step of 30 min. For this work, all simulations were performed using meteorology for the year 2008. A spin-up of one year (i.e. for the year 2007) with the respective meteorology and emissions has been applied.

## *2.2 Simulations and Emission Perturbations*

A number of simulations have been further performed for this study (Table 1) in order to investigate the importance of LRT over the Mediterranean basin, focusing in particular on the EM part. In short, simulations are performed to investigate the impact of regional anthropogenic (MaskANTHRO), biogenic (MaskBIO) and biomass burning (MaskBB) emissions in the EM. The simulation MaskALL neglects all regional emissions to provide information on the background air-quality levels (sustained by mid - and long - range transport to the EM). Note that for the present work, the area between 15°E - 40°E in longitude and 30°N - 45°N in latitude is defined as the EM domain in the model (i.e. 25 longitudinal boxes and 15 latitudinal boxes for the BASE simulation).

Additionally, simulations are performed to separately investigate the impact of LTR from non-EM parts of Europe (MaskEU), North America (MaskNAM), Asia (MaskAS) and Africa (MaskAF) to the EM background atmosphere. For this work, we use the HTAP phase 2 definitions (available online via the HTAP Wiki-page) for the source regions over which emissions are masked. An additional simulation (FUTURE) investigates the impact of future global anthropogenic emissions on EM O<sub>3</sub> levels, based on emission projections for the year 2050 (Stohl et al., 2015). The sensitivity simulations for the investigation of emissions and LTR strength are performed with the computationally cheaper, coarser horizontal resolution configuration of the model (i.e. 6° in longitude by 4° in latitude).

## *2.3 Global model evaluation methodology*

The model's performance has been evaluated by comparing the simulated O<sub>3</sub> and CO levels with surface observations, ozonesonde data and satellite retrievals, all for the year 2008. O<sub>3</sub> surface observations are taken from the European Monitoring Evaluation Program network (EMEP; [www.emep.int](http://www.emep.int)) and from the World Ozone and Ultraviolet Radiation Data Centre (WOUDC; <http://www.woudc.org>) (the location of all surface observational sites used for model evaluation is provided in the supplementary material Table S1 and Fig. S1). Ozonesonde data from sites around the world provided by the WOUDC are used to evaluate the computed vertical structure



of O<sub>3</sub>. CO surface observations around the globe for the year 2008 are taken from World Data Centre for Greenhouse Gases (WDCGG; <http://ds.data.jma.go.jp/gmd/wdcgg/>).

TM4-ECPL results for tropospheric O<sub>3</sub> and CO have been further compared with data from the Tropospheric Emission Spectrometer (TES) satellite instrument. TES is a high resolution (0.1 cm<sup>-1</sup>), infrared, Fourier Transform spectrometer aboard the NASA Aura satellite that follows a polar Sun - synchronous orbit with an equator crossing time at 01:45 and 13:45 local time, and has a repeating cycle of 16 days. The version 4 of TES global survey data, focusing on the FT region of 800-400 hPa, are used here following the methods presented by Voulgarakis et al. (2011). The TES products are provided in 67 levels in the vertical with a varying layer thickness and with an averaged nadir footprint of 5 km by 8 km (Beer, 2006). Model 3-hourly output is sampled at the times and locations of the TES measurements. The model values are logarithmically interpolated onto the 67 TES pressure levels in the vertical, and the TES a priori profiles and averaging kernels are applied. The processed observational and model data are regridded to a 3°x2° grid (in longitude by latitude horizontal resolution).

To quantify the model's ability in simulating O<sub>3</sub> and CO levels, statistical parameters commonly used for model validation have been calculated: the correlation coefficient (R), the standard error (STD), the normalized mean bias (NMB), the normalized mean error (NME) and the root mean square error (RMSE). In short, R reflects the strength of the linear relationship between model results and observations (the ability of the model to simulate the observed variability), and it is insensitive to either an additive or a multiplicative factor; STD is a numerical value indicating the reliability of the mean, estimated by the sample standard deviation divided by the square root of the sample size; MNE and MNB indicate the errors and biases towards overestimations; RMSE is a measure of mean relative scatter reflecting both systematic and random errors. All equations used for the statistical analysis of model results are provided in the supplementary material (Eq. S1-S5).

## *2.4 Budget Calculations*

To calculate the pollutant budget, the atmosphere has been divided into three vertical zones; the boundary layer (BL; from the surface up to 850hPa – the 6 first levels of the model), the free troposphere (FT; between 850hPa and the tropopause –the next 13 levels of the model) and the stratosphere (ST; from the tropopause up to the top of the model's atmosphere 0.1hPa – the top

15 levels of the model). Pollutant lateral fluxes through the boundaries of the studied region have been calculated for these three vertical zones as well as vertical exchange fluxes between the BL and the FT and between the FT and the ST. Emissions, chemical production, chemical destruction and deposition have also been computed for the budget analysis. The tropopause in the model is here determined by the lowest grid boxes where monthly mean O<sub>3</sub> concentrations are greater than 150 ppb<sub>v</sub> (i.e. the chemical tropopause as in Stevenson et al., 2006). The chemical production of O<sub>3</sub>, which occurs through the oxidation of CO, CH<sub>4</sub>, and NMVOCs in the presence of NO<sub>x</sub>, is here computed as the sum of the change in O<sub>3</sub> concentration due to chemistry (net chemical production) and the O<sub>3</sub> chemical loss computed as the sum of the reactions that destroy O<sub>3</sub>. These are O<sub>3</sub> photolysis followed by the reaction of the produced excited oxygen atom with water vapour to form OH radical and O<sub>3</sub> reactions with alkenes, hydrogen peroxy and hydroxyl radicals (for the reactions see Myriokefalitakis et al., 2008). All budget terms are calculated every model time step and averaged/integrated appropriately. Lifetimes are calculated by dividing the burden with the respective loss budget term.

### 3. Results and discussion

Evaluation of the factors that control surface O<sub>3</sub> and CO levels as reflected in atmospheric air quality modeling is critical for air-quality strategies while an accurate simulation of vertical profiles is important for O<sub>3</sub> climate forcing calculations. In this respect, first the simulated distributions of O<sub>3</sub> and CO for the year 2008 are evaluated and then their budget over the Mediterranean and the impact of specific sources to the surface air pollution levels are discussed.

#### 3.1 Evaluation of O<sub>3</sub> and CO distributions

##### 3.1.1 Evaluation of Surface O<sub>3</sub>

To compare observations with model results, EMEP stations have been first divided into four groups, representing different regions of Europe; namely: a) Northwestern Europe (45°N – 60°N; 10°W - 15°E), b) Northeastern Europe (45°N - 60°N; 15°E - 40°E), c) Southwestern Europe (30°N - 45°N; 10°W - 15°E) and d) Southeastern Europe (30°N - 45°N; 15°E - 40°E). Monthly model results are interpolated for each station's coordinates and averaged separately for each group to provide monthly mean surface concentrations of all stations for each of the 4 different European domains (Fig. 1). Note that the number of stations varies between regions and that for

each region the monthly observational data and the respective standard errors as well as model calculations (for every station's coordinates) have been averaged appropriately.

Fig. 1a shows that for the Northwestern European domain, the model overestimates the available observations in summer ( $R=0.8$ ;  $MNB=24\%$ ). The same pattern is simulated for the Northeastern European domain (Fig. 1b;  $R=0.9$ ;  $NMB=27.2\%$ ) where the model also overestimates observed  $O_3$  in summer. For both, the Southeastern and the Southwestern parts of Europe (Fig. 1d and Fig. 1c, respectively), TM4-ECPL satisfactorily reproduces the observed variability of concentrations ( $R=0.8$ ) but with a general tendency to overestimate Southwestern Europe surface  $O_3$  in summer (up to 60 ppb<sub>v</sub> in summer,  $NMB=21.8\%$ , while much smaller overestimate is found for Southeastern Europe;  $NMB=7.5\%$ ). However, the general summertime model overestimation of surface  $O_3$  compared to observations implies a potentially strong photochemical  $O_3$  production calculated by the model, especially in the Western part of the Mediterranean, where the model predicts  $O_3$  concentrations for the period from May to September that are higher than the 84.1 percentile ( $+1\sigma$ , standard deviation) of the measurements (Fig. 1c). These discrepancies can be attributed to the inaccuracies in emissions of  $O_3$  precursors and to the model's coarse resolution that implies limited accuracy of non-linearities in chemistry (Kanakidou and Crutzen, 1999). Another possible reason of the departure of  $O_3$  simulated concentrations from observations during summer is the simulation of the dry deposition  $O_3$  flux.

Simulated surface  $O_3$  is further evaluated on a global scale against available surface observations from the WOUDC, for the year 2008. Fig. S2a presents the point-by-point (scatter plot) of all available measurements from WOUDC and EMEP stations. Observed  $O_3$  mixing ratios are generally well reproduced by the model ( $R=0.7$ ,  $RSME = 11.9$  ppb<sub>v</sub>), but the model in general tends to overestimate the observations ( $MNB = 15.2\%$ ).

### *3.1.2 Evaluation of $O_3$ vertical structure*

Ozonesonde observations compiled by the WOUDC have also been used to evaluate the models' capability in reproducing the  $O_3$  observed vertical profiles. Fig. 2 presents the comparison of model results with observations in 2008 at the Hohenpeissenberg (Germany) and Payerne (Switzerland) ozonesonde stations for five pressure levels (900 hPa, 800 hPa, 500 hPa, 400 hPa and 200 hPa), covering boundary layer and the low and high free troposphere. In order to compare with the WOUDC observations, both the model results and the ozonesondes

observations have been firstly linearly interpolated into layers of 50 hPa from the surface to the top of the atmosphere. Comparisons for the other European stations available by WOUDC (i.e. Lindenber – Germany; Legiovo – Poland; De Bilt – The Netherlands; Ankara – Turkey) are further presented in the supplementary material (Fig. S3). The model captures the O<sub>3</sub> distribution quite well almost at all sites throughout the lower troposphere. Differences in the model performance at the various stations can be due to the different characteristics of the stations, for instance the O<sub>3</sub> precursor source regions, the intensity of photochemistry and the major transport patterns that are affecting them. Above 200hPa model overestimations are mainly attributed to the upper boundary conditions applied in the model (see Section 2.1). The point-by-point comparison of monthly mean values for all WOUDC ozonesonde tropospheric observations sites for the year 2008 (2344 pairs) is also presented in Fig. S2b. Globally, the model overestimates observations by roughly 20% (R = 0.8, NMB = 10.6%, NME 20%). Similar performance is also found over Europe (Fig. S2b).

### *3.1.3 Evaluation of Free Tropospheric O<sub>3</sub> Concentrations*

Simulated O<sub>3</sub> concentrations are further compared to the TES satellite retrievals for the middle/low FT. Fig. 3a depicts the annual mean calculated O<sub>3</sub> concentrations between 800 and 400 hPa (the vertical region with the maximum TES instrument sensitivity) over Europe calculated by TM4-ECPL and Fig. 3c shows the percentage difference from TES retrievals. The model tends to overestimate the mean free tropospheric O<sub>3</sub> concentrations retrieved from TES observations over Northern Europe and Scandinavia (up to 3%), while simulated O<sub>3</sub> concentrations are underestimated up to 5% in the EM.

Fig. S4 also shows the seasonality in the zonal mean (60°S – 60°N) O<sub>3</sub> concentrations in the free troposphere (800 - 400hPa) as computed by the model and its difference from the TES observations. This comparison reveals an O<sub>3</sub> overestimate by the model (up to about 10%) in the northern high latitude regions during the summer months and an underestimate in lower latitudes that reaches 15% in the tropics during NH spring-summer. However, it is worth to note here that the disagreement between TM4-ECPL and TES could be partially explained by the observed TES positive bias between 3-10 ppbv (Nassar et al., 2008).

### 3.1.4 Evaluation of surface CO concentrations

TM4-ECPL results have also been compared with surface CO observations from the WDCGG database for the year 2008. Fig. 4 presents the CO comparison of monthly mean model results with observations for countries within Europe; although the number of the CO monitoring stations is limited (8 stations for the year 2008 over Europe). For this comparison, monthly model results have been extracted for each station and an average for all stations in the same country has been obtained. Fig. 4 shows that the model satisfactorily simulates the CO surface concentrations for Germany ( $R = 0.7$ , NMB = -4.9%), Slovenia ( $R = 0.6$ , NMB = -2.8%) and Switzerland ( $R = 0.6$ , NMB = -3.3%), while an offset is found for the station in The Netherlands ( $R = 0.9$ , NMB = -26.6%). The model evaluation for all CO surface observational sites over Europe and the globe for the year 2008 is also presented in Fig. S2c, based on monthly mean values. The point-by-point global comparison shows that the model generally underestimates the observations (NMB = -21%) but captures the variability ( $R = 0.9$ ).

### 3.1.5 Evaluation of Free Tropospheric CO concentrations

Simulated CO concentrations in the lower free troposphere are also compared with the TES products. Fig. 3b depicts the annual mean CO concentrations between 800-400 hPa over Europe calculated by TM4-ECPL and Fig. 3d shows the percentage difference between the model results and the CO TES product for 2008. The model underestimates the annual mean CO concentrations over Europe by about 10%. The seasonality of the zonal mean CO concentrations between 60°S and 60°N in the middle/low free troposphere (800-400hPa) as calculated by TM4-ECPL is presented in Fig. S4b. The model calculates a winter and a spring maximum in the Northern Hemisphere (NH), and less than half concentrations in the Southern Hemisphere. Secondary maxima due to biomass burning processes are also simulated for the tropics from August to February. The model tends to underestimate CO summer concentrations in the NH. In the NH subtropics (0° – 30°N) the model underestimation of CO concentrations reaches almost 20% from April to late June (Fig. S4d). On the contrary, the model tends to overestimate the retrieved CO tropospheric concentrations by about 10% in the mid-latitudes from September to December. Note however, that studies of TES CO products validation against aircraft data have shown a small bias of TES products that was slightly negative (<10 %) in mid-latitudes and slightly positive (<10 %) in the tropics (Luo et al., 2007; Lopez et al., 2008). Thus, some TM4-ECPL disagreement (Fig. S4f) can be attributed to observational errors. The tendency to

underestimate northern extratropical CO and to overestimate tropical CO in the free troposphere is, however, a common feature in current atmospheric modelling (e.g. Naik et al., 2013).

## 3.2 Tropospheric budget analysis for O<sub>3</sub> and CO

### 3.2.1 Global troposphere

Global tropospheric burden for O<sub>3</sub> and CO governed by both sources (i.e., the chemical production and the stratosphere-troposphere exchanges for O<sub>3</sub>, and emissions and chemical production for CO) and sinks (chemical destruction and deposition for both O<sub>3</sub> and CO) have been calculated for the year 2008. Large O<sub>3</sub> chemical production (5294 Tg yr<sup>-1</sup>) and chemical destruction (5031 Tg yr<sup>-1</sup>) terms are calculated, while dry deposition flux (753 Tg yr<sup>-1</sup>) and stratospheric net influx (490 Tg yr<sup>-1</sup>) are computed to be an order of magnitude lower. These values are well in the range of the 26 model results that participated in the Stevenson et al. (2006) model intercomparison study for the year 2000 (chemical production of  $5110 \pm 606$  Tg yr<sup>-1</sup>, a chemical destruction of  $4668 \pm 727$  Tg yr<sup>-1</sup>, a dry deposition flux of  $1003 \pm 200$  Tg yr<sup>-1</sup> and a stratospheric influx of  $552 \pm 200$  Tg yr<sup>-1</sup>). Similarly, the mean tropospheric O<sub>3</sub> burden of 345 Tg here calculated is close to the  $344 \pm 39$  Tg O<sub>3</sub> tropospheric burden derived by Stevenson et al. (2006).

For the year 2008 in the TM4-ECPL, global CO primary emissions amount 896 Tg yr<sup>-1</sup>, global CO chemical production is calculated to be 1946 Tg yr<sup>-1</sup> that is about twice the primary emissions and chemical destruction to be 2647 Tg yr<sup>-1</sup>. The total CO source (i.e. emissions and chemical production, 2427 Tg yr<sup>-1</sup> for 2008) is in agreement with earlier studies; e.g. about 2760 Tg yr<sup>-1</sup> for the year 1997 derived by Müller and Stavrakou (2005) using inverse modeling calculated the global CO source and 2455 Tg yr<sup>-1</sup> calculated by Kanakidou and Crutzen (1999). The chemical destruction of CO in the model is due to the oxidation by OH radicals. OH radical oxidation is also the primary loss mechanism for methane (CH<sub>4</sub>) and for this OH atmospheric burden is commonly studied simultaneously to CH<sub>4</sub> chemical lifetime. For the year 2008, the TM4-ECPL calculates a tropospheric chemical lifetime of CH<sub>4</sub> of about 8.1 years, which is close to the low-end of mean tropospheric chemical CH<sub>4</sub> lifetime due to OH oxidation for the year 2000, as derived from the ACCMIP (Atmospheric Chemistry and Climate Modeling Intercomparison Project) multi-model mean ( $9.8 \pm 1.6$  yr; Voulgarakis et al., 2013). CO tropospheric burden calculated by TM4-ECPL is 317 Tg for the year 2008, similar to the

estimate by Kanakidou and Crutzen (1999) and by 20% lower than the 397 Tg calculated by Müller and Stavrou (2005). However, the dry deposition sink calculated both by Bergamaschi et al. (2000) (288 Tg yr<sup>-1</sup>) and by Müller and Stavrou (2005) (186-205 Tg yr<sup>-1</sup>) is larger than the deposition flux of about 172 Tg yr<sup>-1</sup> calculated by TM4-ECPL.

### 3.2.2 Eastern Mediterranean

Fig. 5 and Fig. 6 sketch the budget calculations over the Mediterranean, for O<sub>3</sub> and for CO respectively, separating also the Western from the Eastern basin (shaded/non - shaded areas) and the BL (lower parts) from the FT (upper parts). For the BASE simulation, in the EM-BL O<sub>3</sub> is imported from the North (5 Tg yr<sup>-1</sup>), from the western boundary (20 Tg yr<sup>-1</sup>) and from the EM-FT aloft (36 Tg yr<sup>-1</sup>) and exported mainly to the South (38 Tg yr<sup>-1</sup>) and to the East (24 Tg yr<sup>-1</sup>). This result further indicates the significance of free tropospheric O<sub>3</sub> intrusions for the EM O<sub>3</sub> abundance in the BL. Photochemistry in the EM-BL (involving NO<sub>x</sub>, VOCs photo-oxidation) acts as an additional significant source for O<sub>3</sub> in the region with a net chemical production calculated to about 12 Tg yr<sup>-1</sup>. For CO, the model calculates for the EM-BL a burden of 0.6 Tg of CO, a chemical production of 10 Tg yr<sup>-1</sup>, primary emissions in the region of 8 Tg yr<sup>-1</sup> and a dry deposition flux of 3 Tg yr<sup>-1</sup>. Free-tropospheric intrusion imports 22 Tg yr<sup>-1</sup> of CO to the EM-BL and 20 Tg yr<sup>-1</sup> of CO are advected from the west. The model also calculates a strong CO outflow of 32 Tg yr<sup>-1</sup> to the South and a weaker import from the northern boundary that accounts about 6 Tg yr<sup>-1</sup>.

As far as it concerns the EM-FT (Fig. 5 and Fig. 6; upper parts), significant amounts of O<sub>3</sub> and CO are advected through the western boundary (383 Tg yr<sup>-1</sup> and 228 Tg yr<sup>-1</sup>, respectively) and even larger amounts are exported due to chemical build-up and LRT to the East (445 Tg yr<sup>-1</sup> and 240 Tg yr<sup>-1</sup>, respectively). Three times higher O<sub>3</sub> burden over the EM (2.1 Tg) is simulated in the FT than the BL, while O<sub>3</sub> residence time over the EM is calculated to be about 2.7 days in the BL and about 1.5 days in the FT. The model simulates a net O<sub>3</sub> photochemical source of 3 Tg yr<sup>-1</sup> and a CO net chemical destruction of about 4 Tg yr<sup>-1</sup> in the EM-FT. Subsidence from higher atmospheric layers is an important source for both O<sub>3</sub> (48 Tg yr<sup>-1</sup>) and CO (12 Tg yr<sup>-1</sup>) in the EM-FT. Moreover, northern winds enriched in O<sub>3</sub> and CO carry significant amounts of these pollutants to the region's FT (39 Tg yr<sup>-1</sup> and 25 Tg yr<sup>-1</sup>, respectively), while about 17 Tg yr<sup>-1</sup> of O<sub>3</sub> are also imported from the southern boundary to the EM-FT, partly resulting from transport from Asia and Africa (17% and 16% respectively).

### 3.2.3 Western Mediterranean and comparison to the Eastern basin

Fig. 5 and Fig. 6 (shaded area) also depict  $O_3$  and CO budgets in the Western Mediterranean (WM). TM4-ECPL calculates a significant influence from the surroundings since advection of pollutants into the WM-FT (sum of all import terms) is about 2 orders of magnitude higher than the net photochemical source in this region.

The WM-BL is receiving 4 times lower amounts of  $O_3$  from the FT ( $9 \text{ Tg yr}^{-1}$ ) than the Eastern basin, and the chemical production of  $O_3$  ( $36 \text{ Tg yr}^{-1}$ ) is slightly lower than that for EM. According to TM4-ECPL model calculations, stratospheric  $O_3$  intrusions are an important source ( $75 \text{ Tg yr}^{-1}$ ) of tropospheric  $O_3$  over the entire Mediterranean. However, over the WM smaller  $O_3$  amounts are computed (roughly 36% of the total stratospheric intrusions), due to the stagnant conditions in the BL (Millán et al., 2005) as compared to the EM, even though an  $O_3$  burden of about  $2.1 \text{ Tg}$  in the WM-FT is also calculated as for the case of EM-FT. In the WM-BL, the  $O_3$  chemical lifetime is calculated to be about 12.7 days while the overall residence time in the western basin is estimated at about 4.7 days (i.e. about 33% longer than that in the EM) due to deposition and fast outflow. Ventilation by advection is about 3 times faster in the EM than in the WM (about 4 days versus 12 days, respectively). However, the chemical lifetime of  $O_3$  in the BL is almost identical in the two basins (about 12 days) while the subsidence from the FT is about 4 times higher in the EM than in the WM. Overall, the EM-BL is acting as a receptor of  $O_3$  of air masses mainly from the FT (59%) and the WM (33%), as well as a source of  $O_3$  and CO for the downwind locations to the South (60%) and the East (40%). Air-masses advected from the North are about 2 times richer in  $O_3$  in the WM-FT than in the EM-FT, even though the subsidence from the stratosphere provides about 78% more  $O_3$  in the EM-FT than in the WM-FT.

### 3.3 Contribution of sources to air pollution

TM4-ECPL calculations show that the Mediterranean (Fig. 7c) is among the regions experiencing the highest surface  $O_3$  concentrations in the globe together with eastern U.S. and Central Asia (Fig. 7a). In general, TM4-ECPL calculates high surface  $O_3$  concentrations in the mid-latitudes of the NH, over regions with high anthropogenic activity (US, Europe and China) as well as in the tropical areas affected by biomass burning emissions (Fig. 7a). The zonal mean distribution of  $O_3$  concentrations (not shown) presents enhanced values in the sub-tropics



because of O<sub>3</sub> production in regions affected by biomass burning such as Central Africa. The model also calculates high O<sub>3</sub> concentrations in the pollution plumes over the Atlantic and the outflow over Japan.

Simulated surface CO also shows enhanced concentrations over polluted regions of the NH (i.e. US, Europe and China) as well as the biomass burning peaks over Central Africa and the Amazon Basin (Fig. 7b). Although, primary CO sources are mainly from anthropogenic origin (roughly 60%), CO secondary sources from VOC oxidation are calculated to be by 70% from CH<sub>4</sub> and by 30% from NMVOCs (e.g. Poisson et al., 2000). The CO zonal mean distribution (not shown) clearly shows the high NH concentrations, resulting from both high primary and secondary sources north of 30°S. TM4-ECPL calculates higher CO concentrations in the winter (not shown) mainly due to the lower loss by reaction with OH that presents a seasonal wintertime minimum in the troposphere (reduced oxidizing capacity).

In order to investigate the contribution of local and distant sources to air pollution in the BL, emission perturbation simulations have been performed and compared to the base case simulation (BASE) as previously explained in Section 2.2. Percent differences were calculated as  $100 \times (\text{BASE} - \text{MaskX}) / \text{BASE}$ ; where MaskX is the respective sensitivity simulation as presented in Table 1.

### *3.3.1 O<sub>3</sub> surface concentrations*

The model (BASE) calculates a surface annual O<sub>3</sub> mean mixing ratio of about 43 ppb<sub>v</sub> over the European domain in the model (Fig. 7c), with a maximum exceeding 55 ppb<sub>v</sub> over the central and Eastern Mediterranean. The calculations attribute up to 15% of the O<sub>3</sub> surface concentrations to the regional anthropogenic emissions in the EM (MaskAnthro vs. BASE), with an annual mean contribution in the EM of about 8% (Fig. 8a). Additionally, up to 5% on an annual basis is associated with biogenic emissions (MaskBIO vs. BASE), but less than 1% is due to biomass burning emissions (MaskBB vs. BASE). All regional emissions accounted by the model (MaskALL vs. BASE) are responsible for about 11% of O<sub>3</sub> surface levels on annual base, with a maximum contribution of 18% over and south of the Levantine Sea (Fig. 8c), indicating thus the importance of air-mass transport from neighboring regions (i.e. LRT by advection and subsidence to the region). When European emissions are neglected (MaskeU vs. BASE), the model calculates about 13% of reduction in O<sub>3</sub> surface concentrations over the EM (Fig. S5a).

Northern America's emissions (Fig. S5b) affect the surface O<sub>3</sub> concentrations over the entire European continent by about 5% (MaskNAM vs. BASE). Asian emissions (MaskAS vs. BASE) affect O<sub>3</sub> surface concentrations by 10% on annual basis (Fig. S5c), while the African continent's emissions (MaskAF vs. BASE) contribute about 4% to EM basin surface O<sub>3</sub> concentrations (Fig. S5d).

### 3.3.2 CO surface concentrations

For CO concentrations over Europe, the model calculates a surface annual mean mixing ratio of 110 ppb<sub>v</sub>, with a maximum concentration of 128 ppb<sub>v</sub> over EM (Fig. 7d). Anthropogenic local emissions in the EM contribute by 18% to the surface CO levels in the EM (Fig. 8b) annually. Maximum anthropogenic contribution (roughly 32%) to surface CO concentrations is calculated over Cairo. On the other hand, CO concentrations over the EM are associated by about 9% on annual basis with regional biogenic VOC oxidation (not shown) and about 3% are due to biomass burning emissions (not shown). All regional emissions accounted by the model (Fig. 8d) are responsible for 23% of CO surface levels, while the remaining could be attributed to LRT. On an annual basis, European emissions (MaskEU) contribute by about 25% to the calculated CO surface concentrations over the EM (Fig. S6a), Northern America's emissions (MaskNAM) by 12% (Fig. S6b), Asian emissions (MaskAS) by 26% (Fig. S6c) and African emissions (MaskAF) by 11% (Fig. S6d).

### 3.4 Projected changes due to anthropogenic emissions

In Fig. 8e and 8f, the simulation using anthropogenic emissions as projected for the year 2050 (FUTURE) is compared to the BASE (i.e.  $100 \times (\text{FUTURE} - \text{BASE}) / \text{BASE}$ ). A 16% increase in surface O<sub>3</sub> over central Europe is due to the reduction in NO<sub>x</sub> anthropogenic emissions (a reduction in the NO<sub>x</sub> O<sub>3</sub>-titration effect), while a decrease in surface O<sub>3</sub> by about 11% is calculated for the Mediterranean (Fig. 8e) is due to the reduction in O<sub>3</sub> chemical formation and to import/export fluxes changes. On the opposite, CO surface concentrations are calculated to decrease by about 10% over central Europe. This change is the overall effect of the decrease (more than 40%) in the primary anthropogenic emissions, an almost similar in magnitude increase in the OH radical concentrations (affecting both the secondary CO source and the chemical sink of CO) and changes in the transport fluxes. The opposite trend is projected for the EM, where an increase (Fig. 8f) by about 10% in CO surface concentrations is computed. This

change reflects mainly the increase of CO primary anthropogenic emissions in the south combined with a reduction in surface OH levels by about 20% (e.g. due to smaller precursor O<sub>3</sub> concentrations) that leads to a reduction in both the secondary source and in the chemical sink of CO in the EM.

All FUTURE O<sub>3</sub> imports compared to the BASE simulation (computed as  $[100 \times (\text{FUTURE} - \text{BASE}) / \text{BASE}]$ ) due to advection to EM-BL are calculated to decrease roughly by 13% on average, with the Northern boundaries imports to decrease, however, by about 17%. On the other hand, exports from the EM-BL are also calculated to decrease under 2050 anthropogenic emissions, mainly to the South (14%). Note that the same decrease is also calculated for the EM-FT, resulting thus to a decrease in downdraft to EM-BL of about 13%. As far as it concerns the CO, in the EM-BL increases in CO imports from the EM-FT boundary and from the West (about 24% and 17%, respectively) are calculated. In contrast, a decrease in import from the North of about 14% is also calculated for EM-BL, which can also be attributed to impact of Asian emissions as discussed in the previous section (Section 3.3.2). CO has a longer lifetime compared to O<sub>3</sub>, which makes the LRT Asian contribution to European pollution more pronounced on CO than on O<sub>3</sub> within Europe (i.e. Fig. S6c). For the FUTURE simulation, both meteorology and CH<sub>4</sub> concentrations are kept constant in the model, thus the increase in CO chemical production and destruction is attributed to the respective increase in O<sub>3</sub> levels and thus in OH production, leading to a more aggressive CO loss. As explained in section 2.1 changes in meteorology and the stratospheric boundary conditions, which may occur in the future under climate change, are not taken into account by the model. Thus, the computed anti-correlation between O<sub>3</sub> and CO future changes over the EM is driven by the changes in anthropogenic emissions and the induced differences in the oxidation capacity.

#### 4. Conclusions

The global chemistry-transport model TM4-ECPL is able to reproduce observations of O<sub>3</sub> and CO at the surface, the BL and in FT in the rural and remote atmosphere over Europe. This allowed us to analyze the O<sub>3</sub> and CO budget over the EM. We found that the EM atmosphere is strongly affected by air masses from surrounding regions and thus by sources other than local. Similar conclusions for the EM, documented in different ways, have been reached by other modeling studies (e.g. Im and Kanakidou, 2012; Zanis et al., 2014) as well as in the reviews by Kanakidou et al. (2011) and Kallos et al. (2013) and references therein. In the present study we

further quantified the contribution of various sources to the O<sub>3</sub> and CO budget in the EM. In particular, our calculations show that local anthropogenic emissions are responsible for about 8% of surface O<sub>3</sub> concentration and 18% of CO surface concentrations, while downward transport from the FT provides about 38% of O<sub>3</sub> sources and about 33% of CO sources into the EM-BL and horizontal advection from the surrounding regions contributes by about 51% and 27%, respectively. Therefore, neglecting all the emissions in the EM region (i.e. anthropogenic, biomass burning, biogenic and natural emissions) leads to a reduction in annual mean surface concentrations of only 11% in O<sub>3</sub> and of 23% in CO.

For anthropogenic emissions projected for the year 2050, the model calculates a reduction of about 11% in the regional O<sub>3</sub> surface concentrations, with a contemporaneous increase in CO surface concentrations of roughly 10% in the EM. The opposite changes of O<sub>3</sub> and CO due to future anthropogenic emissions could be attributed to the respective changes of oxidation capacity within the EM and to changes in the fluxes in and out the EM which are driven by large-scale concentration changes. However, our calculations do not account for potential changes in meteorology and stratospheric boundary conditions. Overall, this work indicates that O<sub>3</sub> and CO surface levels in the EM are mainly driven by LRT of pollution and related precursors within the BL, but also through the FT and subsequent downdraft to the BL. This implies that mitigation of local anthropogenic emissions is not sufficient for significant improvements in air quality in the Mediterranean region, and that coordinated efforts between the countries surrounding and located upwind of the basin are required.

## 537 **Acknowledgements**

538 This work has been initiated in the frame of the CityZEN project (megaCITY - Zoom for the  
539 Environment, FP7-ENV-2008-212095) and has been finalized with support to SM and GSF by  
540 ECLIPSE (Evaluating the CLimate and Air Quality ImPacts of Short-livEd Pollutants, FP7-  
541 ENV-2011-282688) and to ND by PEGASOS (Pan - European Gas - AeroSOls - climate  
542 interaction Study, FP7-ENV-2010-265148) collaborative projects funded by the European  
543 Commission. We thank Prof. N. Mihalopoulos and Dr. G. Kouvarakis for Finokalia station data  
544 availability and the World Ozone and Ultraviolet Radiation Data Centre (WOUDC) for  
545 ozonesondes data availability.

546

## 547 **References**

- 548 Ainsworth, E.A., Yendrek, C.R., Sitch, S., Collins, W.J., Emberson, L.D., 2012. The effects of  
549 tropospheric ozone on net primary productivity and implications for climate change. *Annu.*  
550 *Rev. Plant Biol.* 63, 637–61. doi:10.1146/annurev-arplant-042110-103829
- 551 Beekmann, M., Vautard, R., 2010. A modelling study of photochemical regimes over Europe:  
552 Robustness and variability. *Atmos. Chem. Phys.* 10, 10067–10084. doi:10.5194/acp-10-  
553 10067-2010
- 554 Beer, R., 2006. TES on the aura mission: scientific objectives, measurements, and analysis  
555 overview. *IEEE Trans. Geosci. Remote Sens.* 44, 1102–1105.  
556 doi:10.1109/TGRS.2005.863716
- 557 Bergamaschi, P., Hein, R., Heimann, M., Crutzen, P.J., 2000. Inverse modeling of the global CO  
558 cycle: 1. Inversion of CO mixing ratios. *J. Geophys. Res.* 105, 1909.  
559 doi:10.1029/1999jd900818
- 560 Brohede, S., McLinden, C.A., Urban, J., Haley, C.S., Jonsson, A.I., Murtagh, D., 2008. Odin  
561 stratospheric proxy NO<sub>y</sub> measurements and climatology. *Atmos. Chem. Phys.* 8, 5731–  
562 5754. doi:10.5194/acp-8-5731-2008
- 563 Colette, A., Granier, C., Hodnebrog, Ø., Jakobs, H., Maurizi, A., Nyiri, A., Rao, S., Amann, M.,  
564 Bessagnet, B., D'Angiola, A., Gauss, M., Heyes, C., Klimont, Z., Meleux, F.,  
565 Memmesheimer, M., Mieville, A., Rouil, L., Russo, F., Schucht, S., Simpson, D., Stordal,  
566 F., Tampieri, F., Vrac, M., 2012. Future air quality in Europe: a multi-model assessment of  
567 projected exposure to ozone. *Atmos. Chem. Phys.* 12, 10613–10630. doi:10.5194/acp-12-  
568 10613-2012
- 569 Crutzen, P.J., 1974. Photochemical reactions initiated by and influencing ozone in unpolluted  
570 tropospheric air. *Tellus* 26, 47–57. doi:10.1111/j.2153-3490.1974.tb01951.x
- 571 Daskalakis, N., Myriokefalitakis, S., Kanakidou, M., 2015. Sensitivity of tropospheric loads and  
572 lifetimes of short lived. *Atmos. Chem. Phys.* 15, 3543–3563. doi:10.5194/acp-15-3543-  
573 2015
- 574 Dee, D.P., Uppala, S.M., Simmons, A.J., Berrisford, P., Poli, P., Kobayashi, S., Andrae, U.,  
575 Balmaseda, M.A., Balsamo, G., Bauer, P., Bechtold, P., Beljaars, A.C.M., van de Berg, L.,  
576 Bidlot, J., Bormann, N., Delsol, C., Dragani, R., Fuentes, M., Geer, A.J., Haimberger, L.,  
577 Healy, S.B., Hersbach, H., Hólm, E. V., Isaksen, I., Kållberg, P., Köhler, M., Matricardi,  
578 M., McNally, A.P., Monge-Sanz, B.M., Morcrette, J.J., Park, B.K., Peubey, C., de Rosnay,  
579 P., Tavolato, C., Thépaut, J.N., Vitart, F., 2011. The ERA-Interim reanalysis: configuration  
580 and performance of the data assimilation system. *Q. J. Roy. Meteor. Soc.* 137, 553–597.  
581 doi:10.1002/qj.828
- 582 Derwent, R.G., Jenkin, M.E., Saunders, S.M., 1996. Photochemical ozone creation potentials for  
583 a large number of reactive hydrocarbons under European conditions. *Atmos. Environ.* 30,  
584 181–199. doi:10.1016/1352-2310(95)00303-G
- 585 Drori, R., Dayan, U., Edwards, D.P., Emmons, L.K., Erlick, C., 2012. Attributing and  
586 quantifying carbon monoxide sources affecting the Eastern Mediterranean: a combined  
587 satellite, modelling, and synoptic analysis study. *Atmos. Chem. Phys.* 12, 1067–1082.  
588 doi:10.5194/acp-12-1067-2012
- 589 Eckhardt, S., Quennehen, B., Olivié, D.J.L., Berntsen, T.K., Cherian, R., Christensen, J.H.,

- Collins, W., Crepinsek, S., Daskalakis, N., Flanner, M., Herber, A., Heyes, C., Hodnebrog, Ø., Huang, L., Kanakidou, M., Klimont, Z., Langner, J., Law, K.S., Lund, M.T., Mahmood, R., Massling, A., Myriokefalitakis, S., Nielsen, I.E., Nøjgaard, J.K., Quaas, J., Quinn, P.K., Raut, J.-C., Rumbold, S.T., Schulz, M., Sharma, S., Skeie, R.B., Skov, H., Uttal, T., Salzen, K. von, Stohl, A., 2015. Current model capabilities for simulating black carbon and sulfate concentrations in the Arctic atmosphere: a multi-model evaluation using a comprehensive measurement data set. *Atmos. Chem. Phys.* 15, 9413–9433. doi:10.5194/acp-15-9413-2015
- Fountoukis, C., Nenes, A., 2007. ISORROPIA II: a computationally efficient thermodynamic equilibrium model for  $K^+$  -  $Ca^{2+}$  -  $Mg^{2+}$  -  $NH_4^+$  -  $Na^+$  -  $SO_4^{2-}$  -  $NO_3^-$  -  $Cl^-$  -  $H_2O$  aerosols. *Atmos. Chem. Phys.* 7, 4639–4659. doi:10.5194/acp-7-4639-2007
- Gerasopoulos, E., Amiridis, V., Kazadzis, S., Kokkalis, P., Eleftheratos, K., Andreae, M.O., Andreae, T.W., El-Askary, H., Zerefos, C.S., 2011. Three-year ground based measurements of aerosol optical depth over the Eastern Mediterranean: the urban environment of Athens. *Atmos. Chem. Phys.* 11, 2145–2159. doi:10.5194/acp-11-2145-2011
- Gerasopoulos, E., Kouvarakis, G., Vrekoussis, M., Kanakidou, M., Mihalopoulos, N., 2005. Ozone variability in the marine boundary layer of the eastern Mediterranean based on 7-year observations. *J. Geophys. Res. D Atmos.* 110, 1–12. doi:10.1029/2005JD005991
- Groß, J.U., Russell III, J.M., 2005. Technical note: A stratospheric climatology for  $O_3$ ,  $H_2O$ ,  $CH_4$ ,  $NO_x$ ,  $HCl$  and  $HF$  derived from HALOE measurements. *Atmos. Chem. Phys.* 5, 2797–2807. doi:10.5194/acp-5-2797-2005
- HTAP, T., 2011. Hemispheric Transport of Air Pollution 2010 Part A: Ozone And Particulate Matter. *Air Pollut. Stud.*
- Im, U., Kanakidou, M., 2012. Impacts of East Mediterranean megacity emissions on air quality. *Atmos. Chem. Phys.* 12, 6335–6355. doi:10.5194/acp-12-6335-2012
- Im, U., Markakis, K., Poupkou, A., Melas, D., Unal, A., Gerasopoulos, E., Daskalakis, N., Kindap, T., Kanakidou, M., 2011. The impact of temperature changes on summer time ozone and its precursors in the Eastern Mediterranean. *Atmos. Chem. Phys.* 11, 3847–3864. doi:10.5194/acp-11-3847-2011
- Jimoda, L., 2012. Effects of particulate matter on human health, the ecosystem, climate and materials: A review. *Facta Univ. Work. Living ...* 9, 27–44.
- Kallos, G., Astitha, M., Katsafados, P., Spyrou, C., 2007. Long-Range Transport of Anthropogenically and Naturally Produced Particulate Matter in the Mediterranean and North Atlantic: Current State of Knowledge. *J. Appl. Meteorol. Climatol.* 46, 1230–1251. doi:10.1175/JAM2530.1
- Kallos, G., Mitsakou, C., Alastuey, A., van Aardenne, J., Astitha, M., Cusack, M., Doering, U., Gerasopoulos, E., Hatzianastassiou, N., Kanakidou, M., Kushta, J., Lelieveld, J., Levin, Z., Mihalopoulos, N., Millán, M., Palau, J.L., Perez, N., Pey, J., Querol, X., Solomos, S., Spyrou, C., Theodosi, C., Zerefos, C., 2013. Mechanisms of Climate Variability, Air Quality and Impacts of Atmospheric Constituents in the Mediterranean Region, in: Navarra, A., Tubiana, L. (Eds.), *Advances in Global Change Research*. Springer Netherlands, Dordrecht, pp. 119–156. doi:10.1007/978-94-007-5781-3\_4
- Kanakidou, M., Crutzen, P.J., 1999. The photochemical source of carbon monoxide: Importance,

- uncertainties and feedbacks. *Chemosph. - Glob. Chang. Sci.* 1, 91–109.  
doi:http://dx.doi.org/10.1016/S1465-9972(99)00022-7
- Kanakidou, M., Mihalopoulos, N., Kindap, T., Im, U., Vrekoussis, M., Gerasopoulos, E.,  
Dermitzaki, E., Unal, A., Koçak, M., Markakis, K., Melas, D., Kouvarakis, G., Youssef,  
A.F., Richter, A., Hatzianastassiou, N., Hilboll, A., Ebojie, F., Wittrock, F., von Savigny,  
C., Burrows, J.P., Ladstaetter-Weissenmayer, A., Moubasher, H., 2011. Megacities as hot  
spots of air pollution in the East Mediterranean. *Atmos. Environ.* 45, 1223–1235.  
doi:10.1016/j.atmosenv.2010.11.048
- Kanakidou, M., Singh, H.B., Valentin, K.M., Crutzen, P.J., 1991. A two-dimensional study of  
ethane and propane oxidation in the troposphere. *J. Geophys. Res.* 96, 15395–15413.  
doi:10.1029/91jd01345
- Langner, J., Engardt, M., Baklanov, A., Christensen, J.H., Gauss, M., Geels, C., Hedegaard,  
G.B., Nuterman, R., Simpson, D., Soares, J., Sofiev, M., Wind, P., Zakey, A., 2012. A  
multi-model study of impacts of climate change on surface ozone in Europe. *Atmos. Chem.*  
*Phys.* 12, 10423–10440. doi:10.5194/acp-12-10423-2012
- Lelieveld, J., Berresheim, H., Borrmann, S., Crutzen, P.J., Dentener, F.J., Fischer, H., Feichter,  
J., Flatau, P.J., Heland, J., Holzinger, R., Korrman, R., Lawrence, M.G., Levin, Z.,  
Markowicz, K.M., Mihalopoulos, N., Minikin, A., Ramanathan, V., De Reus, M., Roelofs,  
G.J., Scheeren, H. a, Sciare, J., Schlager, H., Schultz, M., Siegmund, P., Steil, B.,  
Stephanou, E.G., Stier, P., Traub, M., Warneke, C., Williams, J., Ziereis, H., 2002. Global  
air pollution crossroads over the Mediterranean. *Science* 298, 794–9.  
doi:10.1126/science.1075457
- Lelieveld, J., Dentener, F.J., 2000. What controls tropospheric ozone? *J. Geophys. Res.* 105,  
3531. doi:10.1029/1999JD901011
- Liakakou, E., Bonsang, B., Williams, J., Kalivitis, N., Kanakidou, M., Mihalopoulos, N., 2009.  
C2–C8 NMHCs over the Eastern Mediterranean: Seasonal variation and impact on regional  
oxidation chemistry. *Atmos. Environ.* 43, 5611–5621. doi:10.1016/j.atmosenv.2009.07.067
- Lopez, J.P., Luo, M., Christensen, L.E., Loewenstein, M., Jost, H., Webster, C.R., Osterman, G.,  
2008. TES carbon monoxide validation during two AVE campaigns using the Argus and  
ALIAS instruments on NASA's WB-57F. *J. Geophys. Res.* 113, D16S47.  
doi:10.1029/2007JD008811
- Louis, J.-F., 1979. A parametric model of vertical eddy fluxes in the atmosphere. *Boundary-*  
*Layer Meteorol.* 17, 187–202. doi:10.1007/BF00117978
- Luo, M., Rinsland, C., Fisher, B., Sachse, G., Diskin, G., Logan, J., Worden, H., Kulawik, S.,  
Osterman, G., Eldering, A., Herman, R., Shephard, M., 2007. TES carbon monoxide  
validation with DACOM aircraft measurements during INTEx-B 2006. *J. Geophys. Res.*  
112, D24S48. doi:10.1029/2007JD008803
- Millán, M., Estrela, M., Sanz, M., 2005. Climatic feedbacks and desertification: the  
Mediterranean model. *J. ...* 684–701.
- Molina, L.T., Molina, M.J. (Eds.), 2002. *Air Quality in the Mexico Megacity*, Alliance for  
Global Sustainability Bookseries. Springer Netherlands, Dordrecht. doi:10.1007/978-94-  
010-0454-1
- Monks, P.S., Granier, C., Fuzzi, S., Stohl, A., Williams, M.L., Akimoto, H., Amann, M.,



- 676 Baklanov, A., Baltensperger, U., Bey, I., Blake, N., Blake, R.S., Carslaw, K., Cooper, O.R.,  
677 Dentener, F., Fowler, D., Fragkou, E., Frost, G.J., Generoso, S., Ginoux, P., Grewe, V.,  
678 Guenther, A., Hansson, H.C., Henne, S., Hjorth, J., Hofzumahaus, A., Huntrieser, H.,  
679 Isaksen, I.S.A., Jenkin, M.E., Kaiser, J., Kanakidou, M., Klimont, Z., Kulmala, M., Laj, P.,  
680 Lawrence, M.G., Lee, J.D., Liousse, C., Maione, M., McFiggans, G., Metzger, A., Mieville,  
681 A., Moussiopoulos, N., Orlando, J.J., O'Dowd, C.D., Palmer, P.I., Parrish, D.D., Petzold,  
682 A., Platt, U., Pöschl, U., Prévôt, A.S.H., Reeves, C.E., Reimann, S., Rudich, Y., Sellegri,  
683 K., Steinbrecher, R., Simpson, D., ten Brink, H., Theloke, J., van der Werf, G.R., Vautard,  
684 R., Vestreng, V., Vlachokostas, C., von Glasow, R., 2009. Atmospheric composition change  
685 – global and regional air quality. *Atmos. Environ.* 43, 5268–5350.  
686 doi:10.1016/j.atmosenv.2009.08.021
- 687 Müller, J.-F., Stavrou, T., 2005. Inversion of CO and NO<sub>x</sub> emissions using the adjoint of the  
688 IMAGES model. *Atmos. Chem. Phys.* 5, 1157–1186. doi:10.5194/acp-5-1157-2005
- 689 Myriokefalitakis, S., Daskalakis, N., Mihalopoulos, N., Baker, A.R., Nenes, A., Kanakidou, M.,  
690 2015. Changes in dissolved iron deposition to the oceans driven by human activity: a 3-D  
691 global modelling study. *Biogeosciences* 12, 3973–3992. doi:10.5194/bg-12-3973-2015
- 692 Myriokefalitakis, S., Tsigaridis, K., Mihalopoulos, N., Sciare, J., Nenes, A., Kawamura, K.,  
693 Segers, A., Kanakidou, M., 2011. In-cloud oxalate formation in the global troposphere: a 3-  
694 D modeling study. *Atmos. Chem. Phys.* 11, 5761–5782. doi:10.5194/acp-11-5761-2011
- 695 Myriokefalitakis, S., Vignati, E., Tsigaridis, K., Papadimas, C., Sciare, J., Mihalopoulos, N.,  
696 Facchini, M.C., Rinaldi, M., Dentener, F.J., Ceburnis, D., Hatzianastasiou, N., O'Dowd,  
697 C.D., van Weele, M., Kanakidou, M., 2010. Global Modeling of the Oceanic Source of  
698 Organic Aerosols. *Adv. Meteorol.* 2010, 1–16. doi:10.1155/2010/939171
- 699 Myriokefalitakis, S., Vrekoussis, M., Tsigaridis, K., Wittrock, F., Richter, A., Brühl, C.,  
700 Volkamer, R., Burrows, J.P., Kanakidou, M., 2008. The influence of natural and  
701 anthropogenic secondary sources on the glyoxal global distribution. *Atmos. Chem. Phys.*  
702 *Discuss.* 8, 1673–1708. doi:10.5194/acpd-8-1673-2008
- 703 Naik, V., Voulgarakis, A., Fiore, A.M., Horowitz, L.W., Lamarque, J.-F., Lin, M., Prather, M.J.,  
704 Young, P.J., Bergmann, D., Cameron-Smith, P.J., Cionni, I., Collins, W.J., Dalsøren, S.B.,  
705 Doherty, R., Eyring, V., Faluvegi, G., Folberth, G.A., Josse, B., Lee, Y.H., MacKenzie,  
706 I.A., Nagashima, T., van Noije, T.P.C., Plummer, D.A., Righi, M., Rumbold, S.T., Skeie,  
707 R., Shindell, D.T., Stevenson, D.S., Strode, S., Sudo, K., Szopa, S., Zeng, G., 2013.  
708 Preindustrial to present-day changes in tropospheric hydroxyl radical and methane lifetime  
709 from the Atmospheric Chemistry and Climate Model Intercomparison Project (ACCMIP).  
710 *Atmos. Chem. Phys.* 13, 5277–5298. doi:10.5194/acp-13-5277-2013
- 711 Nassar, R., Logan, J.A., Worden, H.M., Megretskaia, I.A., Bowman, K.W., Osterman, G.B.,  
712 Thompson, A.M., Tarasick, D.W., Austin, S., Claude, H., Dubey, M.K., Hocking, W.K.,  
713 Johnson, B.J., Joseph, E., Merrill, J., Morris, G.A., Newchurch, M., Oltmans, S.J., Posny,  
714 F., Schmidlin, F.J., Vömel, H., Whiteman, D.N., Witte, J.C., 2008. Validation of  
715 Tropospheric Emission Spectrometer (TES) nadir ozone profiles using ozonesonde  
716 measurements. *J. Geophys. Res.* 113, D15S17. doi:10.1029/2007JD008819
- 717 Olivie, D.J.L., 2004. Comparison between archived and off-line diagnosed convective mass  
718 fluxes in the chemistry transport model TM3. *J. Geophys. Res.* 109, D11303.  
719 doi:10.1029/2003JD004036

- 720 Parrish, D.D., Singh, H.B., Molina, L., Madronich, S., 2011. Air quality progress in North  
721 American megacities: A review. *Atmos. Environ.* 45, 7015–7025.  
722 doi:10.1016/j.atmosenv.2011.09.039
- 723 Pausata, F.S.R., Pozzoli, L., Vignati, E., Dentener, F.J., 2012. North Atlantic Oscillation and  
724 tropospheric ozone variability in Europe: model analysis and measurements  
725 intercomparison. *Atmos. Chem. Phys.* 12, 6357–6376. doi:10.5194/acp-12-6357-2012
- 726 Poisson, N., Kanakidou, M., Crutzen, P., 2000. Impact of Non-Methane Hydrocarbons on  
727 Tropospheric Chemistry and the Oxidizing Power of the Global Troposphere: 3-  
728 Dimensional Modelling Results. *J. Atmos. Chem.* 36, 157–230.  
729 doi:10.1023/A:1006300616544
- 730 Quennehen, B., Raut, J.-C., Law, K.S., Ancellet, G., Clerbaux, C., Kim, S.-W., Lund, M.T.,  
731 Myhre, G., Olivie, D.J.L., Safieddine, S., Skeie, R.B., Thomas, J.L., Tsyro, S., Bazureau,  
732 A., Bellouin, N., Daskalakis, N., Hu, M., Kanakidou, M., Klimont, Z., Kupiainen, K.,  
733 Myriokefalitakis, S., Quaas, J., Rumbold, S.T., Schulz, M., Cherian, R., Shimizu, A., Wang,  
734 J., Yoon, S.-C., Zhu, T., 2015. Multi-model evaluation of short-lived pollutant distributions  
735 over East Asia during summer 2008. *Atmos. Chem. Phys. Discuss.* 15, 11049–11109.  
736 doi:10.5194/acpd-15-11049-2015
- 737 Russell, G.L., Lerner, J.A., 1981. A New Finite-Differencing Scheme for the Tracer Transport  
738 Equation. *J. Appl. Meteorol.* 20, 1483–1498. doi:10.1175/1520-  
739 0450(1981)020<1483:ANFDSF>2.0.CO;2
- 740 Sciare, J., Oikonomou, K., Favez, O., Liakakou, E., Markaki, Z., Cachier, H., Mihalopoulos, N.,  
741 2008. Long-term measurements of carbonaceous aerosols in the Eastern Mediterranean:  
742 evidence of long-range transport of biomass burning. *Atmos. Chem. Phys.* 8, 5551–5563.  
743 doi:10.5194/acp-8-5551-2008
- 744 Stevenson, D.S., Dentener, F.J., Schultz, M.G., Ellingsen, K., van Noije, T.P.C., Wild, O., Zeng,  
745 G., Amann, M., Atherton, C.S., Bell, N., Bergmann, D.J., Bey, I., Butler, T., Cofala, J.,  
746 Collins, W.J., Derwent, R.G., Doherty, R.M., Drevet, J., Eskes, H.J., Fiore, a. M., Gauss,  
747 M., Hauglustaine, D. a., Horowitz, L.W., Isaksen, I.S. a., Krol, M.C., Lamarque, J.-F.F.,  
748 Lawrence, M.G., Montanaro, V., Müller, J.-F.F., Pitari, G., Prather, M.J., Pyle, J. a., Rast,  
749 S., Rodriguez, J.M., Sanderson, M.G., Savage, N.H., Shindell, D.T., Strahan, S.E., Sudo,  
750 K., Szopa, S., 2006. Multimodel ensemble simulations of present-day and near-future  
751 tropospheric ozone. *J. Geophys. Res.* 111, D08301. doi:10.1029/2005jd006338
- 752 Stohl, A., Aamaas, B., Amann, M., Baker, L.H., Bellouin, N., Berntsen, T.K., Boucher, O.,  
753 Cherian, R., Collins, W., Daskalakis, N., Dusinska, M., Eckhardt, S., Fuglestad, J.S.,  
754 Harju, M., Heyes, C., Hodnebrog, Ø., Hao, J., Im, U., Kanakidou, M., Klimont, Z.,  
755 Kupiainen, K., Law, K.S., Lund, M.T., Maas, R., MacIntosh, C.R., Myhre, G.,  
756 Myriokefalitakis, S., Olivie, D., Quaas, J., Quennehen, B., Raut, J.-C., Rumbold, S.T.,  
757 Samset, B.H., Schulz, M., Seland, Ø., Shine, K.P., Skeie, R.B., Wang, S., Yttri, K.E., Zhu,  
758 T., 2015. Evaluating the climate and air quality impacts of short-lived pollutants. *Atmos.*  
759 *Chem. Phys. Discuss.* 15, 15155–15241. doi:doi:10.5194/acpd-15-15155-2015
- 760 Tiedtke, M., 1989. A Comprehensive Mass Flux Scheme for Cumulus Parameterization in  
761 Large-Scale Models. *Mon. Weather Rev.* 117, 1779–1800. doi:10.1175/1520-  
762 0493(1989)117<1779:ACMFSF>2.0.CO;2
- 763 van der A, R.J., Allaart, M. a. F., Eskes, H.J., 2010. Multi sensor reanalysis of total ozone.

764 Atmos. Chem. Phys. 10, 11277–11294. doi:10.5194/acp-10-11277-2010

765 van Noije, T.P.C., Eskes, H.J., van Weele, M., van Velthoven, P.F.J., 2004. Implications of the  
 766 enhanced Brewer-Dobson circulation in European Centre for Medium-Range Weather  
 767 Forecasts reanalysis ERA-40 for the stratosphere-troposphere exchange of ozone in global  
 768 chemistry transport models. J. Geophys. Res. 109, D19308. doi:10.1029/2004JD004586

769 Voulgarakis, A., Naik, V., Lamarque, J.-F., Shindell, D.T., Young, P.J., Prather, M.J., Wild, O.,  
 770 Field, R.D., Bergmann, D., Cameron-Smith, P., Cionni, I., Collins, W.J., Dalsøren, S.B.,  
 771 Doherty, R.M., Eyring, V., Faluvegi, G., Folberth, G.A., Horowitz, L.W., Josse, B.,  
 772 MacKenzie, I.A., Nagashima, T., Plummer, D.A., Righi, M., Rumbold, S.T., Stevenson,  
 773 D.S., Strode, S. a., Sudo, K., Szopa, S., Zeng, G., 2013. Analysis of present day and future  
 774 OH and methane lifetime in the ACCMIP simulations. Atmos. Chem. Phys. 13, 2563–2587.  
 775 doi:10.5194/acp-13-2563-2013

776 Voulgarakis, A., Telford, P.J., Aghedo, a. M., Braesicke, P., Faluvegi, G., Abraham, N.L.,  
 777 Bowman, K.W., Pyle, J. a., Shindell, D.T., 2011. Global multi-year O<sub>3</sub>-CO correlation  
 778 patterns from models and TES satellite observations. Atmos. Chem. Phys. 11, 5819–5838.  
 779 doi:10.5194/acp-11-5819-2011

780 Yue, X., Unger, N., 2014. Ozone vegetation damage effects on gross primary productivity in the  
 781 United States. Atmos. Chem. Phys. 14, 9137–9153. doi:10.5194/acp-14-9137-2014

782 Zanis, P., Hadjinicolaou, P., Pozzer, A., Tyrlis, E., Dafka, S., Mihalopoulos, N., Lelieveld, J.,  
 783 2014. Summertime free-tropospheric ozone pool over the eastern Mediterranean/Middle  
 784 East. Atmos. Chem. Phys. 14, 115–132. doi:10.5194/acp-14-115-2014

785

786

787 **Table 1.** Outline of simulations performed for this study.

<b>Simulation</b>	<b>Description</b>
<b>BASE</b>	The base case simulation for the year 2008.
<b>MaskANTRO</b>	Neglecting the anthropogenic emissions in the Eastern Mediterranean domain.
<b>MaskBB</b>	Neglecting the biomass burning emissions in the Eastern Mediterranean domain.
<b>MaskBIO</b>	Neglecting the biogenic emissions in the Eastern Mediterranean domain.
<b>MaskALL</b>	Neglecting the anthropogenic, biomass burning and biogenic emissions in the Eastern Mediterranean domain.
<b>MaskEU</b>	Neglecting all emissions over Europe.
<b>MaskNAM</b>	Neglecting all emissions over Northern America.
<b>MaskAS</b>	Neglecting all emissions over Asia.
<b>MaskAF</b>	Neglecting all emissions over Africa.
<b>FUTURE</b>	Taking into account projected anthropogenic emission of the year 2050.

788

789

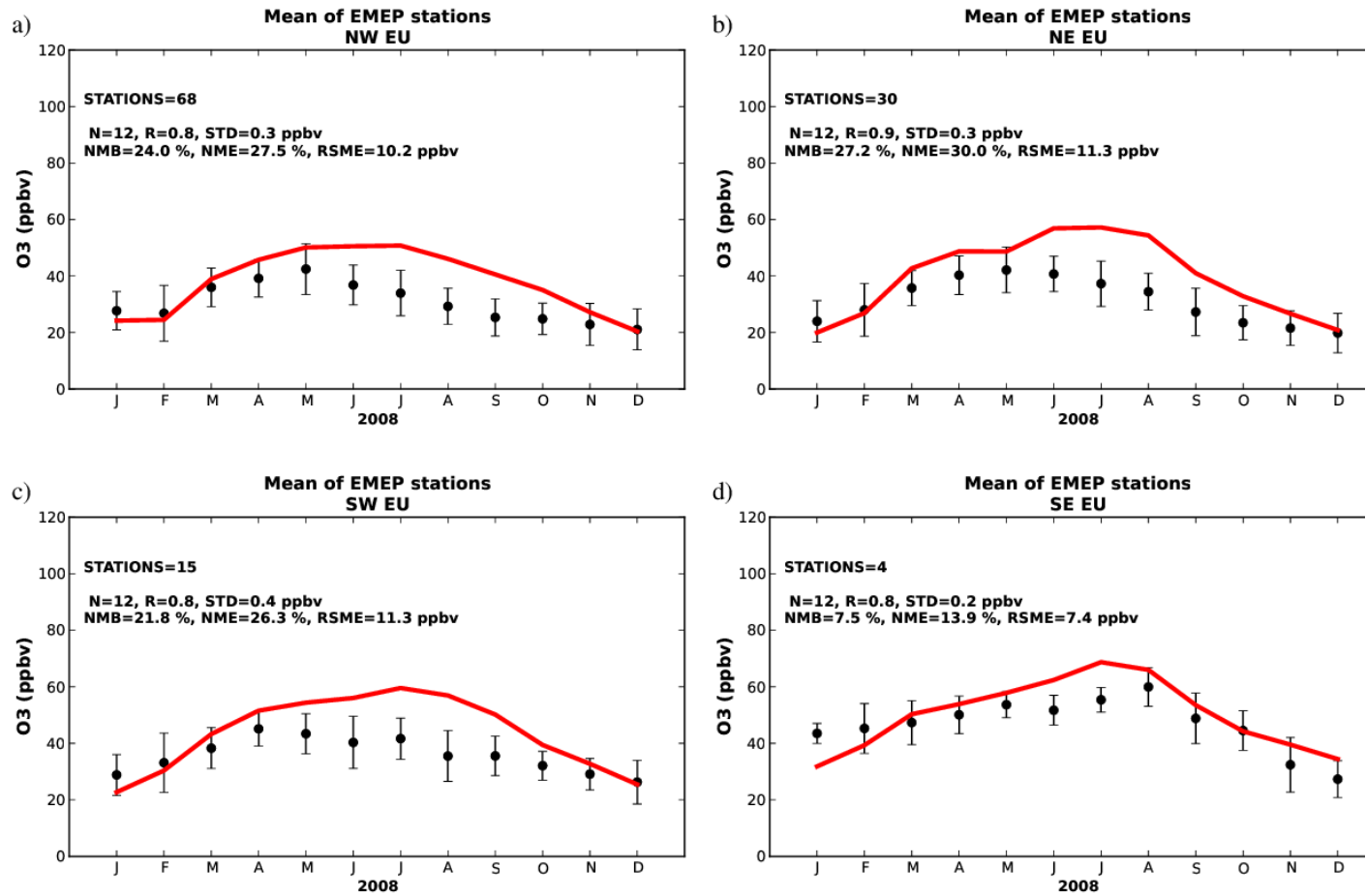


**Fig. 1.** Comparison of O<sub>3</sub> levels (ppb<sub>v</sub>) from TM4-ECPL BASE simulation (red lines) with surface monthly mean observations from EMEP stations (black dots) and the respective standard deviation of the observed O<sub>3</sub> levels (ppb<sub>v</sub>) (with black vertical lines) at a) NW Europe, b) NE Europe, c) SW Europe and d) SE Europe.

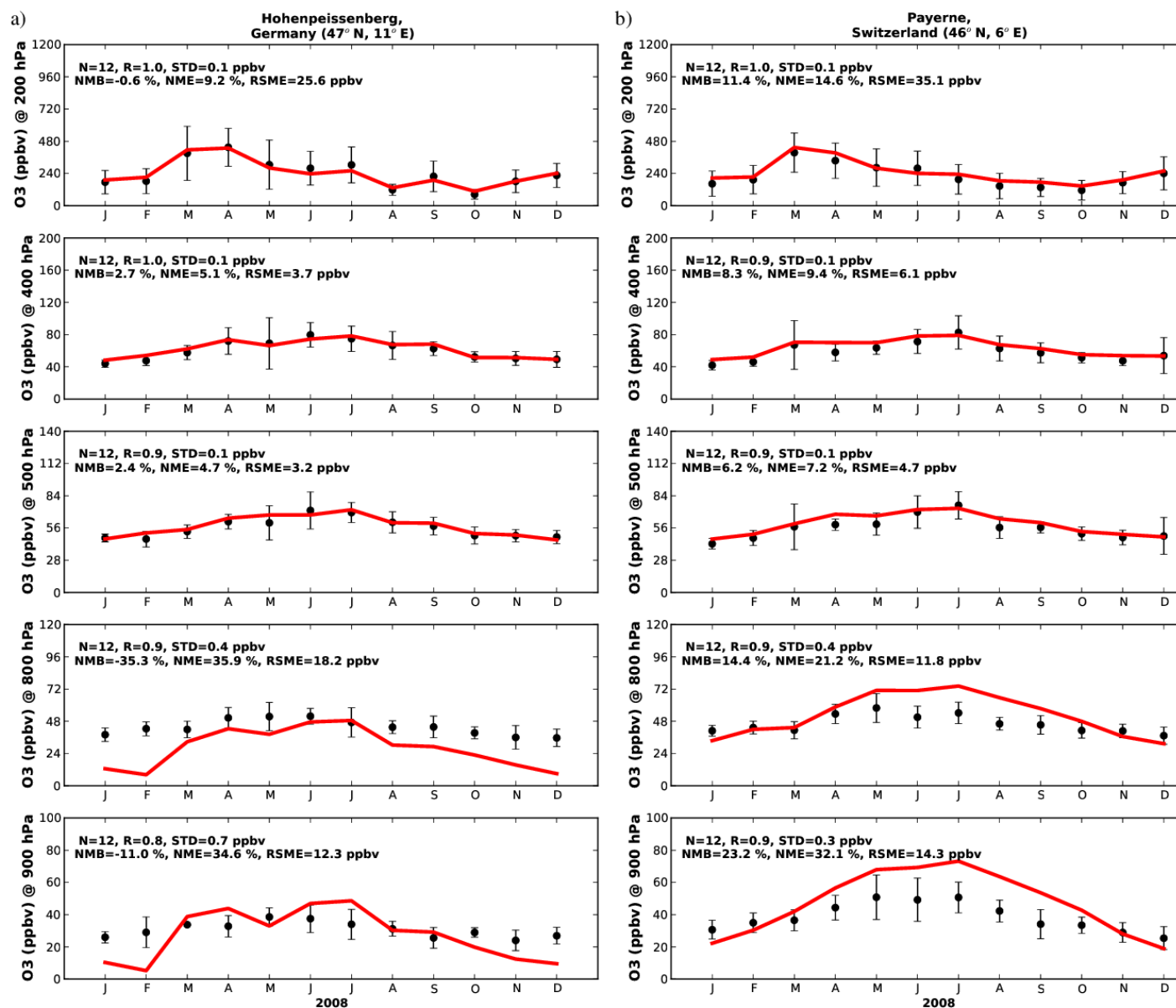


**Fig. 2.** Comparison of O<sub>3</sub> levels (ppbv) from TM4-ECPL BASE simulation (red line) with O<sub>3</sub> sonde station data (black dots, mean and standard deviation) at five pressure levels (900; 800; 500; 400; 200 hPa) for two WOUDC stations: a) Hohenpeissenberg, Germany (47°N, 11°E); b) Payerne, Switzerland (46°N, 6°E) (see additional comparisons at other European stations in Fig. S3 in the supplementary material).

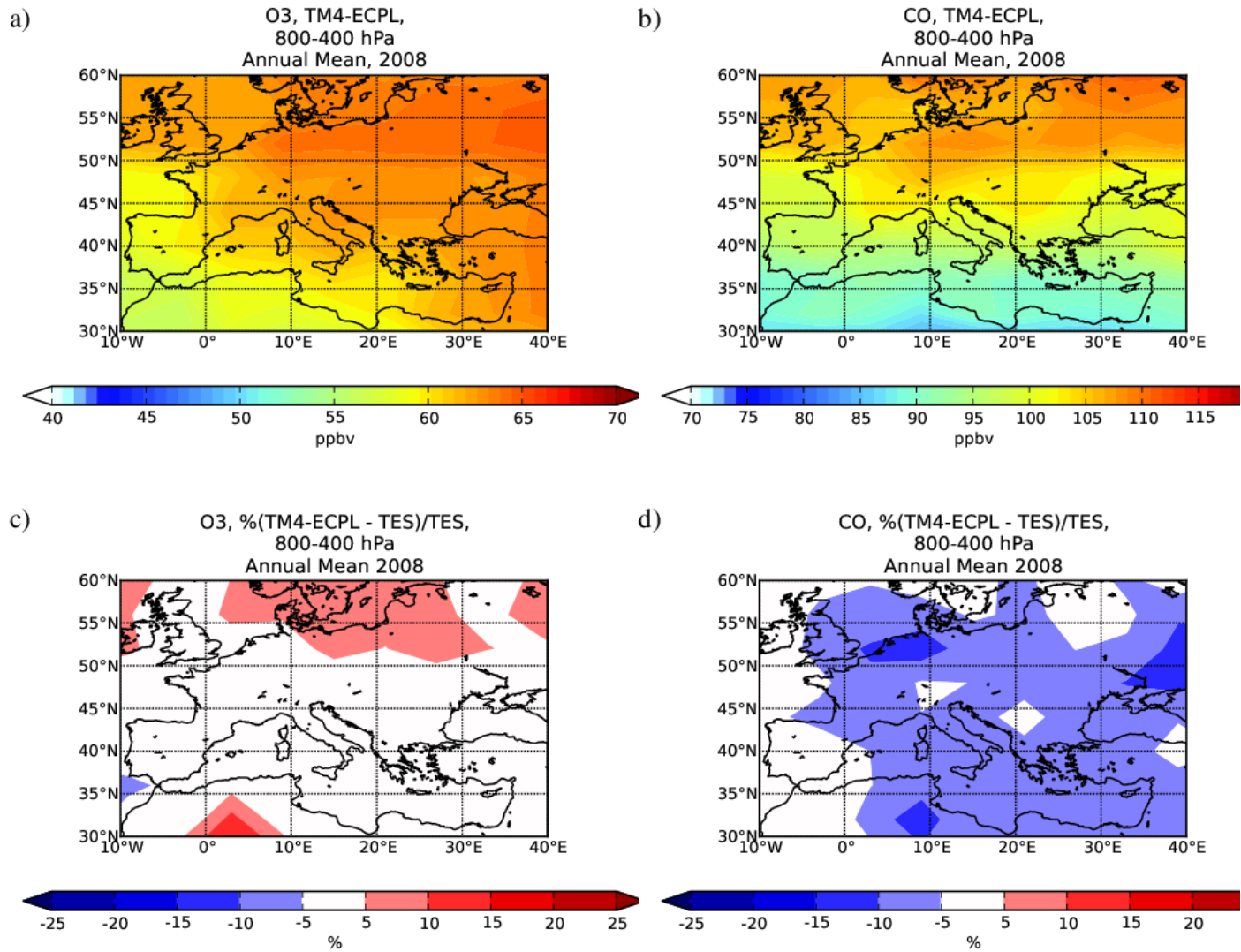


**Fig. 3.** Simulated annual mean free tropospheric concentrations (ppb<sub>v</sub>) in the 800-400 hPa zone over Europe for a) O<sub>3</sub>, b) CO, and the percentage difference of TM4-ECPL BASE simulation results from TES retrieved concentrations [100 x (BASE-TES)/TES] for c) O<sub>3</sub> and d) CO in the same zone.

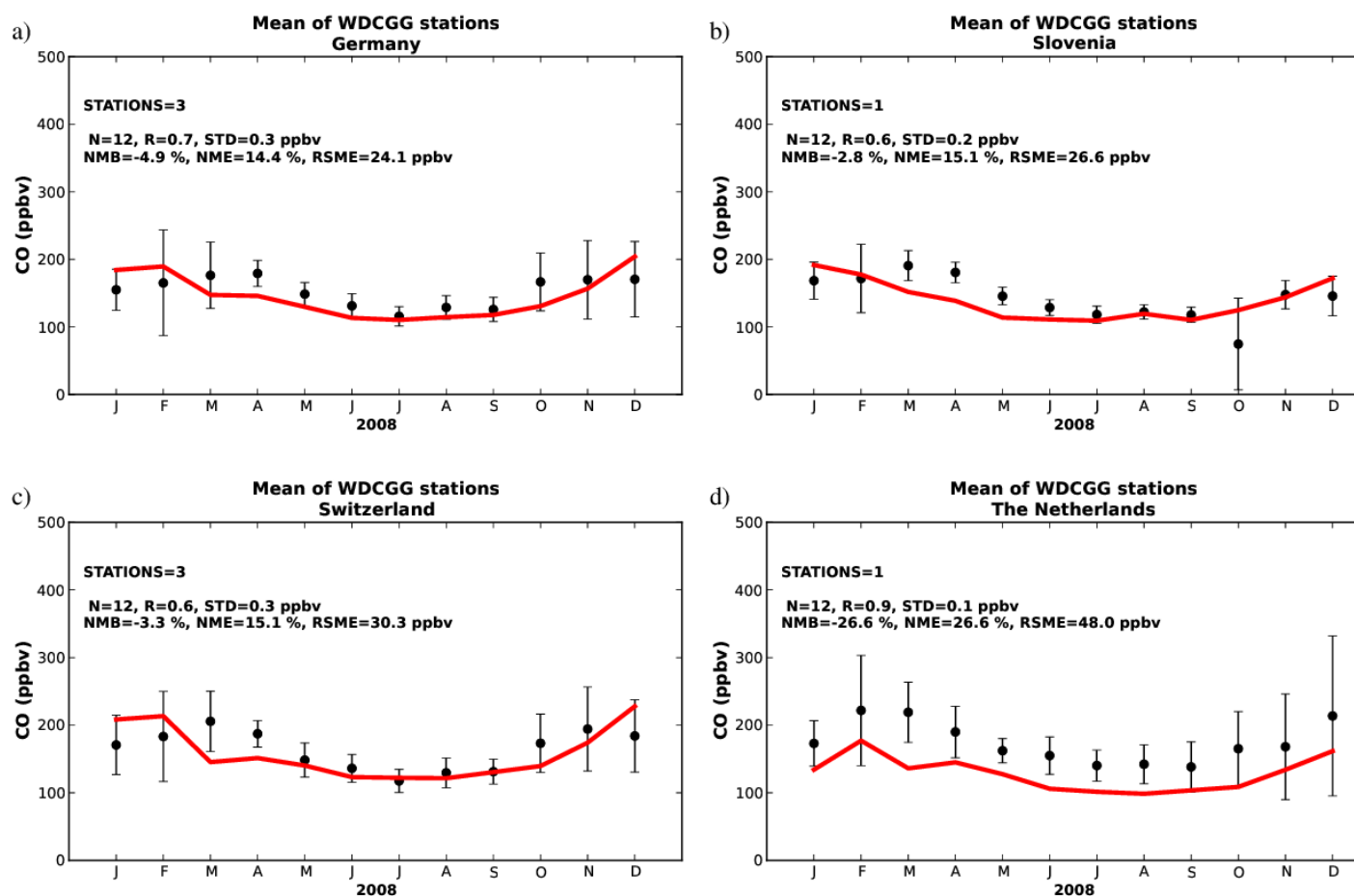


**Fig. 4.** Comparison of surface CO levels (ppbv) calculated by TM4-ECPL BASE simulation (red line) with observations (monthly mean values for WDCGG stations, black dots, mean and standard deviation) at a) Germany, b) Slovenia c) Switzerland and d) The Netherlands



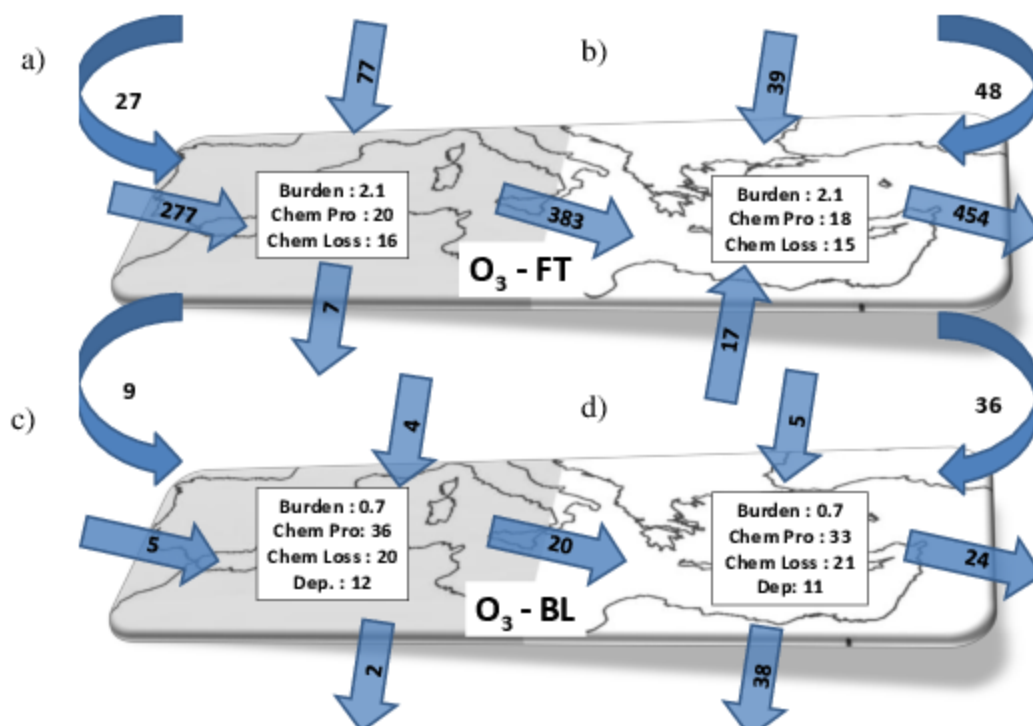


**Fig. 5.**  $O_3$  annual (2008; BASE simulation) budget analysis for Western (a,c; shaded area) and Eastern Mediterranean (b,d; non-shaded area) for a,b) the free troposphere (FT; upper figure) and c,d) the boundary layer (BL; bottom figure) including the burden, the chemistry, the deposition and the fluxes at each boundary. All budget terms and fluxes ( $Tg\ yr^{-1}$ ) are annual totals; burdens ( $Tg$ ) are annual averages. Straight arrows indicate N-S and W-E advection fluxes, while curved arrows indicate vertical fluxes from the upper troposphere to the FT and from the FT to the BL.

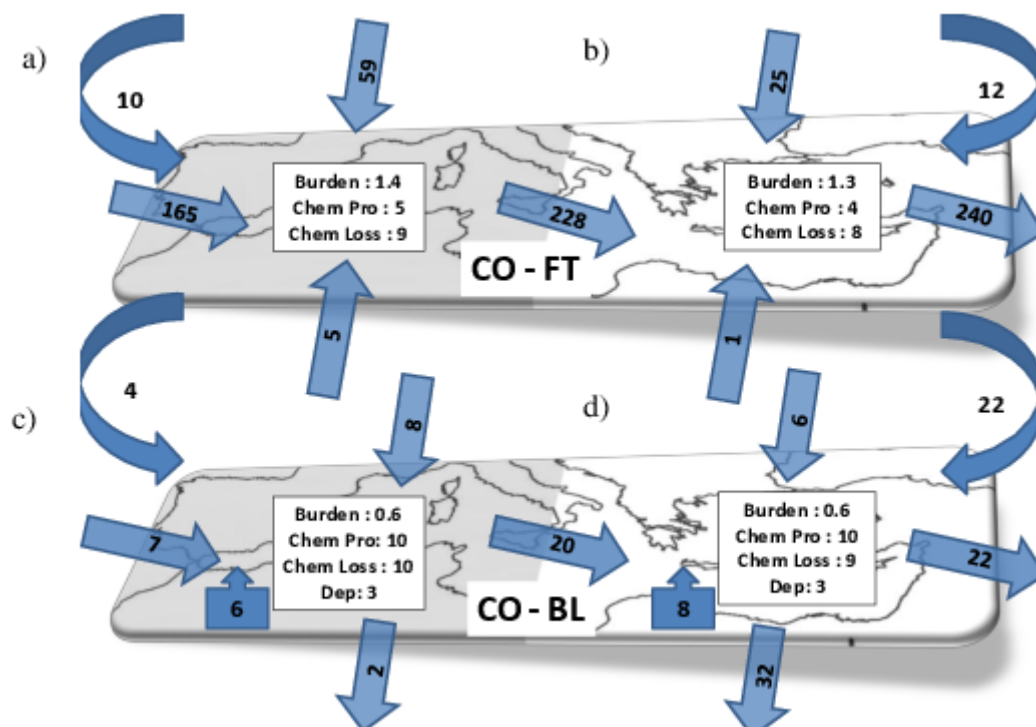


**Fig. 6.** CO annual (2008; BASE simulation) budget analysis for Western (a,c; shaded area) and Eastern Mediterranean (b,d; non-shaded area) for a,b) the free troposphere (FT; upper figure) and c,d) the boundary layer (BL; bottom figure) including the burden, the emissions, the chemistry, the deposition and the fluxes at each boundary.. Straight arrows indicate N-S and W-E advection fluxes, curved arrows indicate vertical fluxes from the upper troposphere to the FT and from the FT to the BL and box-arrows indicate CO emissions.

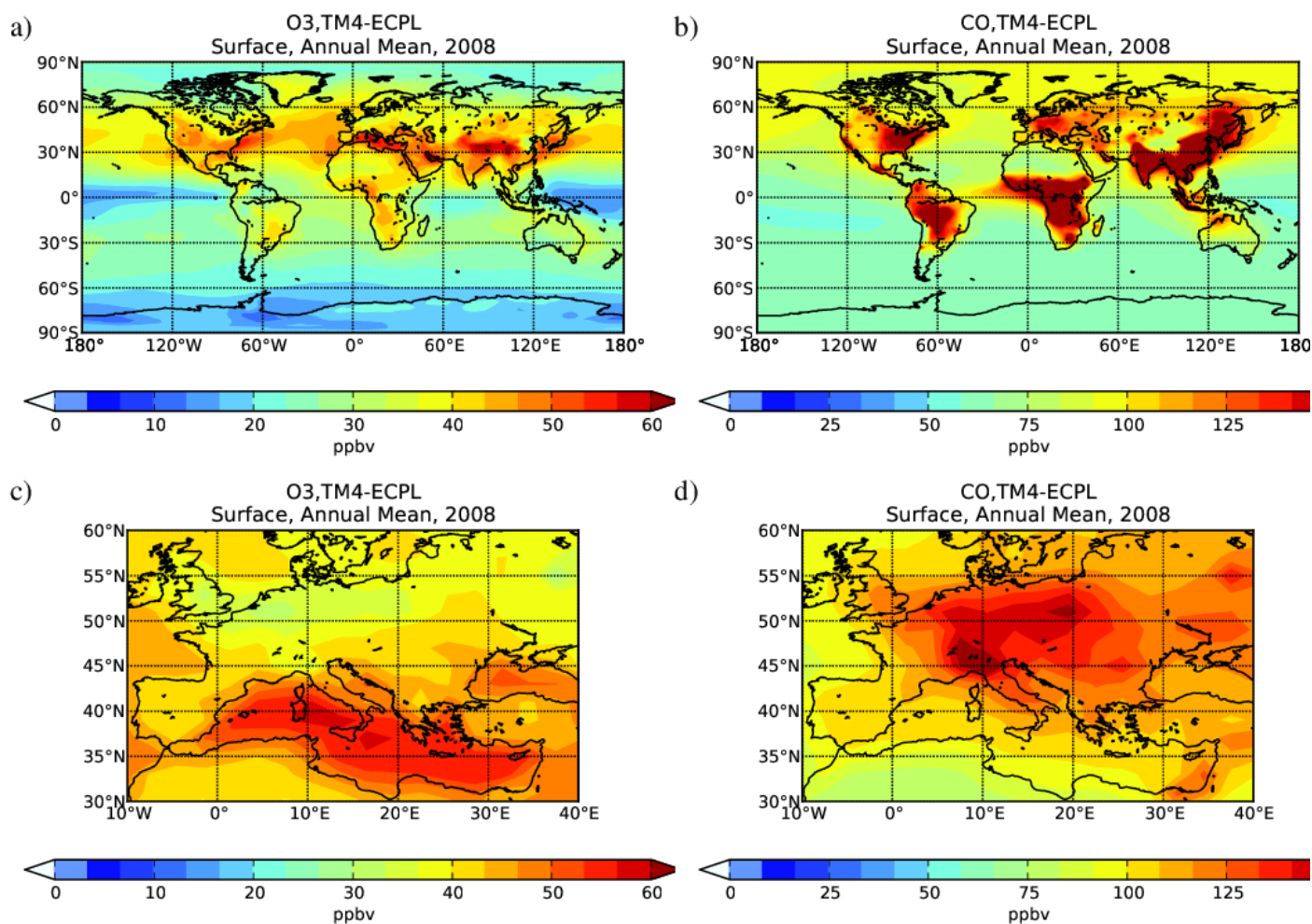


**Fig. 7.** Simulated a,c) O<sub>3</sub> and b,d) CO surface concentrations (ppb<sub>v</sub>) for TM4-ECPL BASE simulation for the globe (a,b) and focus on the Mediterranean area (c,d).

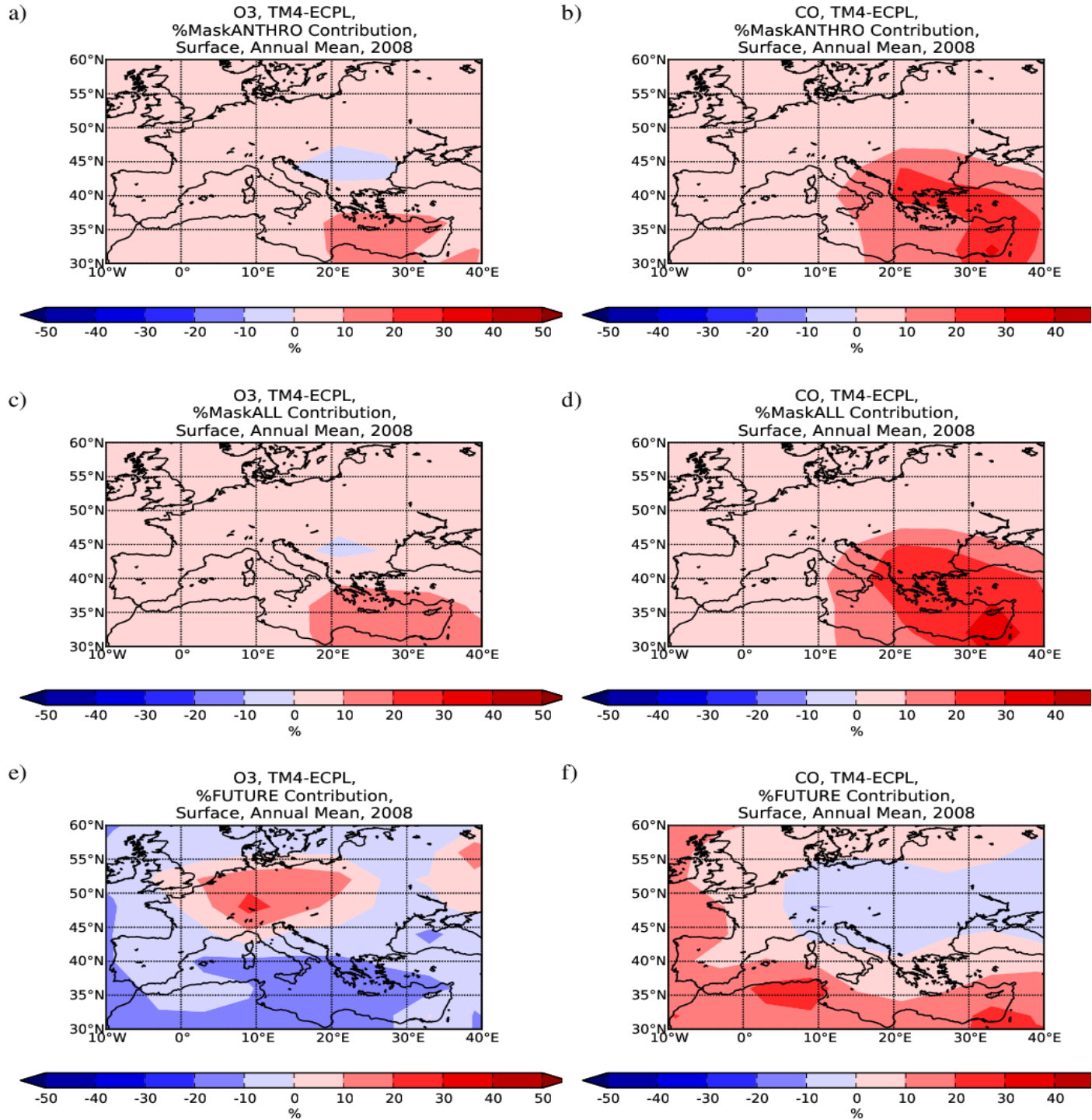


**Fig. 8.** Simulated relative contribution (%) to O<sub>3</sub> (left panels) and CO (right panels) surface concentrations of a,b) Anthropogenic emissions over EM (MaskANTHRO); c,d) All emissions over the EM (MaskALL); and e,f) Future anthropogenic emissions (FUTURE), compared to the TM4-ECPL BASE simulation (figures a) through d) are computed as  $[100 \times (\text{BASE} - \text{MaskX}) / \text{BASE}]$ ; where MaskX is the respective sensitivity simulation, while e) and f) are computed as  $[100 \times (\text{FUTURE} - \text{BASE}) / \text{BASE}]$ .